CHAPTER 3

# SELECTION OF PCM AND ASSESSMENT FOR THERMAL STABILITY AND COMPATIBILITY

# CHAPTER 3

# SELECTION OF PCM AND ASSESSMENT FOR THERMAL STABILITY AND COMPATIBILITY

## 3.1 Introduction

Among the numerous forms of thermal energy storage systems (TESS), latent heat storage (LHS) is considered best due to its wide working temperature range. PCM is classified into three kinds according on the phase change temperatures: (i) low-temperature PCM (phase change temperature of 15 °C, employed in cooling systems and food processing industry). (ii) medium-temperature PCM (phase change temperature greater than 15 °C, employed in solar power, healthcare, textiles electronics, and power-saving architecture designs). (iii) high-temperature PCM (phase change temperature more than 90 °C, used in industrial and aerospace applications) [1]. Medium temperature PCM-TES is advantageous due to several reasons. First, it provides compact energy storage in limited equipment installation space. Second, it provides uniform thermal sink for energy savings and temperature management regardless of the transition to fluctuating renewable energy sources and third, it reduces peak energy demand during high energy usage, cutting production and energy costs [2]. When it comes to medium temperature organic PCMs, paraffin compounds are one of most used PCMs. Organic PCMs are chemically stable, non-corrosive, recyclable, melt uniformly, and require minimal or no supercooling to initiate crystallisation. Organic PCMs have low heat conductivity and store volumetric energy. However, nucleating agents can be used to increase conductivity [3-6]. Important criterion for the PCM selection is discussed thoroughly before and to highlight a few, the PCM having phase change temperature within the desired usage temperature range, high-density, high-specific heat-capacity materials have high energy density, occupying less area with high latent heat fusion, PCMs needed to be quick in melting and solidification to adapt to load fluctuations which means high thermal conductivity. Storage materials with good thermo-chemical characteristics lowers capital cost [7]. It is crucial to undertake research on these features given that the thermo-physical characteristics of the PCMs have a direct effect on the thermal performance of the storage system as well as the cost of the system.

On the other hand, the values of the properties that are described in the published works are typically calculated values rather than values that are experimentally validated, and there usually exists a disparity between these values [8- 10]. Thermal stability and compatibility with container materials are two crucial factors in the effective application of PCMs for TESS. Thermal stability is essential when choosing a PCM for a specific application [11]. Thermogravimetry analysis (TGA) is used to determine the highest limit of thermal stability by understanding the temperature range of a material's thermal degradation. When designing a heat storage unit, long-term material stability is critical. For a given number of cycles, the melting temperature and enthalpy must remain reasonably uniform. As a result, cyclic stability is a critical indicator. Differential scanning calorimeter (DSC) are be used to measure the thermophysical properties of the material [12]. The compatibility between the PCM and the container material must be evaluated. Corrosion is the result of chemical or electrochemical reactions between a PCM and its container material, which, after prolonged exposure to thermal cycling, degrade the container. This natural occurrence cannot be avoided, sadly. Degradation reduces the cross-sectional area of the container materials, rendering them fragile and susceptible to collapse. With a few exceptions, organic PCMs are not naturally corrosive, whereas inorganic compounds are extremely corrosive. Therefore, corrosion testing in numerous temperature ranges is necessary to confirm the compatibility of the container materials with their PCM counterparts for long-term use [13]. The copper, aluminium, and stainless-steel corrosion test evaluated the corrosive behaviour when exposed to six distinct PCMs appropriate for lower temperatures thermal energy storage applications. The compatibility of stainless steel with the chosen PCMs was demonstrated and confirmed to be appropriate [14]. Based on the above discussion and reviews in the earlier Chapter the present Chapter includes.

(a) Identification and selection of PCMs for medium temperature through multi attribute decision making.

(b) Study of long-term thermal stability of the selected PCMs using TGA and DSC techniques.

(c) Study of compatibility of the selected PCMs with the container material or the metal specimens examined by corrosion test, microscopic imaging, and surface roughness profiling.

## 3.2 Materials and methods

### 3.2.1 Scope and goals of PCM selection

The maximum permissible temperature requirement to ensure safe moisture content for preservation of these agricultural produce ranges from 55 ºC to 75 ºC [15]. Therefore, medium temperature PCMs (40 ºC to 90 ºC) are considered for selection of PCM which shall be further studied for thermal stability and compatibility with the container materials. The results of this study will be useful in subsequent research on PCM integration with SAH and solar dryers for valorisation of agricultural products.

### 3.2.2 PCM selection methodology

The first step in the selection approach is to review all the potential PCM candidates available in the literature for heating applications ranging from 40ºC to 90ºC. Given the substantial amount of potential PCM candidates identified in the first step, the second step of the process of selection included a pre-selection to eliminate PCMs that are unsuitable due to possible hazards to health, corrosion with the container material, or extremely poor thermophysical properties, availability, and price of the PCM. Likewise, only the best PCM is selected when two or more had traits in common. One major drawback to using salt hydrates as PCMs is that majority of them melt incongruently.

In particular, when a salt hydrate is melted to a saturated aqueous phase, they crystallise as a lower hydrate of the same salt. Due to density variations, the solid phase of salt hydrate tends to sink to the bottom of the container; this occurrence disqualifies it as a PCM candidate for use in the current investigation.

After narrowing down the list of potential PCM candidates, the third step of the process involves building a decision matrix as a tool to make a final selection based on objective criteria. There is no universally accepted method of selection, thus several criteria may be used depending on the nature of the application. Factors like phase change enthalpy, phase change range breadth, subcooling, hysteresis, thermal conductivity, density, availability, toxicity, and cost are typically considered. Since these characteristics are used to eliminate some of the possible PCM candidates in the selection process, a decision matrix is developed to evaluate the many viable options and find the most promising ones for solar heating application. The decision matrix considered the following factors: maximum operating temperature for PCM integration in solar heating applications, availability, price, melting enthalpy, and width of the phase transition

range. These variables are selected because they have a direct impact on the system's operational and financial viability as well as the relative ease in determining their values. For each PCM candidate, a score is given for each of the choice characteristics, considering the criteria listed in Table 3.1 where 0 to 3 corresponds to score given to each of the parameters by all the selected PCMs. 0 corresponds to least score with lowest thermophysical property values and 3 corresponds to maximum score having highest thermophysical property values.

**Table 3.1:** The scoring criteria applied to each decision parameter

| Parameters | Scoring criteria | Score |
|---|---|---|
| Width of phase change | T<2 | 3 |
| Range, T (ºC) | 2<T<3 | 2 |
| | 3<T<4 | 1 |
| | T>4 or n.a. | 0 |
| Enthalpy, h(kJ/kg) | h>250 | 3 |
| | 200<h<250 | 2 |
| | 150<h<200 | 1 |
| | h<150 or n.a. | 0 |
| Availability | Yes | 3 |
| | No | 0 |
| Price, P (INR/kg) | P < 100 | 3 |
| | 100<P<300 | 2 |
| | 300<P<500 | 1 |
| | P> 500 or n.a. | 0 |
| Maximum operating | $T_{max}$ > 120 | 3 |
| temperature, $T_{max}$ (ºC) | $T_{max}$<120 or n.a. | 0 |

Next, a final score for each PCM is calculated using a weighted average of the partial scores obtained for each of the decision parameters. Table 3.2 displays two scenarios that are considered in terms of the values selected for the weight, with Scenario A displaying the value of each decision parameter selected based on the criteria of the authors based on their experience, and Scenario B displaying the same weight assigned to all decision parameters. Scenario A's parameter weights are set so that the system's primary needs, such as compactness and cost-effectiveness of the TES solution, are addressed, with PCM enthalpy and price being given more weight than the other choice parameters. Each obtained combination's total score is multiplied by the average score of the PCM

candidates that had previously been selected for use in solar heating application, and the top three PCMs in each scenario are selected based on the ranking.

**Table 3.2:** Reference values of the weights

| Decision Parameter | Weight (%) | |
|---|---|---|
| | Scenario A | Scenario B |
| Phase change width Cp-T curve) | 15 | 20 |
| Enthalpy | 30 | 20 |
| Availability | 10 | 20 |
| Price | 30 | 20 |
| Maximum working temperature | 15 | 20 |
| Total | 100 | 100 |

### 3.2.3 Thermal stability analysis of the selected PCMs

The selected PCMs thermal, chemical, and physical stability, depends on its behaviour when employing number of repeated heat cycles, to determine PCM's long term reliability. Methodology utilized to characterize the selected PCMs are discussed below.

#### 3.2.3.1 Thermogravimetric analysis (TGA)

The TGA test is deemed to be necessary as it provides information on the degradation temperature of the sample beyond which the sample decomposes. The uses of TGA for thermal decomposition and degradation study of PCM and composites materials are reported earlier [16-20]. The present study uses Netzsch TG 209 F1 to record mass loss and hence thermal degradation of fresh paraffin wax and stearic acid samples. A fresh sample (10 mg) is heated from 25 ºC to 350 ºC for paraffin wax, 25 ºC to 290 ºC for stearic acid and (6 mg) for acetamide is heated from 25 to 220 ºC under $N_2$ atmosphere with heating rate of 10 ºC/min. Nitrogen gas is used to isolate the effects of degradation and avoid any misleading oxidation reactions. The decomposition temperature is determined using TG curves that display the mass changes with increasing temperature up to 350 ºC for paraffin wax, 290 ºC for stearic acid and 220 ºC for acetamide respectively.

#### 3.2.3.2 Differential scanning calorimetry (DSC)

The differential scanning calorimeter, or DSC, is the equipment of choice in laboratories for measuring the melting temperature and heat of fusion of PCM materials. DSC is a thermo-analytical technique that measures the difference in heat required to raise the

temperature of a sample and a reference as a function of temperature. Both the sample and the reference are kept at virtually the same temperature throughout the experiment. The heat capacity of the reference sample should be well characterised over the temperature range of interest.

The accelerated thermal cycle test (melting and solidifying cycle) of Paraffin wax, stearic acid and acetamide sample is performed to study the thermal stability viz., onset melting temperature, peak melting temperature and latent heat of fusion using DSC (DSC-60 plus Shimadzu, temperature, and enthalpy precision of ±0.5 ºC and ±0.2 %).

The experimental setup for accelerated thermal cycling test comprises of an electrical hot plate (Symax India), glass beaker (inner diameter of 65 mm and height 95 mm). The hot plate (240 V, 50/60 Hz, 6.2 A, 1500 W) has temperature controller with operating range between 25ºC and 300ºC (precision ± 2 ºC). The beakers are filled with 30 g of acetamide, Paraffin wax and stearic acid is heated using hot plate maintained at 120 ºC till the PCM melts completely. Subsequently the beaker is removed from the hotplate for solidification at room temperature to complete one melting and solidification cycle of PCM. The process is repeated for 1000 cycles of melting and solidification while collecting 0.6 g of acetamide, Paraffin wax and stearic acid from the beaker at every 100 cycles for generating DSC thermograph within set temperature between 25 ºC and 150 ºC with the heating rate of 10 ºC/ min. The relevant parameters such as (i) onset melting temperature, (ii) phase transition/peak temperature, (iii) latent heat of fusion is estimated for the thermographs corresponding to each 100th cycle using standard procedure [21,22]. The changes in melting temperature and latent heat of fusion of acetamide during thermal cycling are another aspect of investigation. The values obtained from the DSC thermographs are used to estimate relative percentage difference (RPD, %) using Eq. (1) as provided below.

$$RPD\% = \frac{Xi - X0}{X0} \times 100\% \qquad (3.1)$$

where *Xo* is the relevant parameter (onset melting temperature, phase transition temperature, peak temperature, and latent heat of fusion) at 0th cycle and *Xi* is the relevant parameter at $i^{th}$ cycle. RPD is estimated for each 100th cycle up to 1000 thermal cycles.

### 3.2.4 Compatibility study of metal containers with selected PCMs

For the purpose of ensuring the long-term dependability of the latent heat thermal energy storage (LHTES), it is extremely important to investigate on the compatibility of the PCM with the container elements. Presently the compatibility of PCM with the container materials are investigated with corrosion test which involves prolonged exposure of metal samples with the PCM materials under thermal cycling test and study of mass loss and degradation visually and experimentally.

#### 3.2.4.1 Corrosion test

The corrosion test is conducted for selected metal specimens (aluminium, stainless steel, mild steel, and copper) treated with stearic acid, paraffin wax and acetamide as shown in Fig. 3.1, 3.2 and 3.3. The thermal cycling for up to 1000 repeated cycles is performed to determine the corrosion rate of each metal specimen.

The corrosion characteristics of aluminium, copper, mild steel, and stainless steel on treatment with stearic acid and paraffin wax are studied by gravimetric analysis method as a function of mass loss *(*$\Delta m$) and corrosion rate (*CR*) [23]. The weight loss from the metal samples is calculated using the formula given by Eq. (2) as below.

$$\Delta m = m(t_0) - m(t) \tag{3.2}$$

where, m($t_o$) and m($t$) are the initial and final mass of the metal specimens.

The corrosion rate is calculated with respect to the mass loss *(*$\Delta m$), surface area of metal specimens ($A_m$) and time of exposure of the metal samples ($t$). Corrosion rate of the metal specimens is calculated using the formula given by Eq. (3) as below.

$$CR = \frac{m(t_0) - m(t)}{A_m . t} \tag{3.3}$$

where, the surface area of aluminium is 28 $cm^2$, mild steel is 25.92 $cm^2$, stainless steel is 25.75 $cm^2$ and copper is 28 $cm^2$ respectively. The time of exposure, t is 0.208219 year (76 days) for 1000 thermal cycles in case of stearic acid and paraffin wax. In case of acetamide the surface area of aluminium is 13 $cm^2$, mild steel is 13 $cm^2$, stainless steel is 14 $cm^2$ and copper is 13 $cm^2$ respectively and the time of exposure in acetamide, t is 0.4438 year (162 days) for 1000 thermal cycles.


**Fig. 3.1:** Corrosion test of metal strips (a) aluminium (b) stainless steel (c) mild steel (d) copper with Stearic acid up to 1000 thermal cycling test

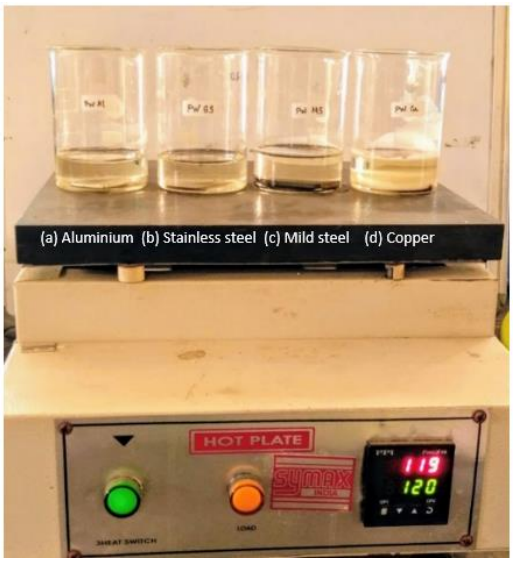


**Fig. 3.2:** Corrosion test of meatal strips (a) aluminium (b) stainless steel (c) mild steel (d) copper with Paraffin wax up to 1000 thermal cycling test

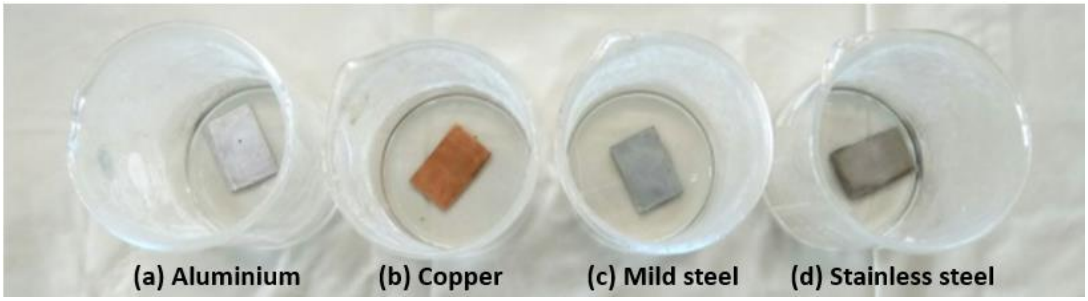


**Fig. 3.3:** Corrosion test of metal strips (a) aluminium (b) copper (c) mild steel (d) stainless steel with acetamide up to 1000 thermal cycling test

### 3.2.4.2 Microscopic imaging and surface roughness study

ZEISS Stemi 305 Stereomicroscope as shown in Fig. 3.4 is used to observe and record the conditions (metallographic study) of the surfaces of the four metal specimens before and after the thermal cycling test while treated with stearic acid, paraffin wax and acetamide respectively. Lenses of the Stereomicroscope camera is adjusted to capture best possible views of the surfaces displaying corrosion, pitting, cracks, etc. In addition to the images captured for visual examination, a surface roughness tester, Surtronic S-128 (Taylor Hobson, range of vertical displacement: 10 nm to 1 mm) as shown in Fig. 3.5 is used to measure the roughness of the metal surfaces before and after treatment with stearic acid, paraffin wax and acetamide respectively. The profilometer measurement provides the intensity of etching and corrosive deposition on the surfaces of the samples by two important parameters, roughness average *($R_a$)* and maximum peak-to-valley height *($R_t$)* respectively.

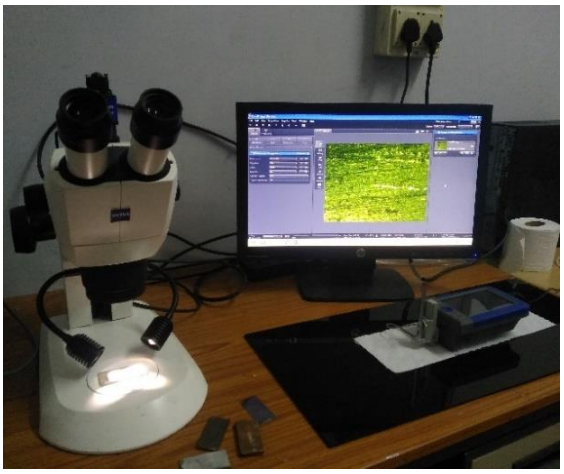

**Fig. 3.4:** Microscopic imaging of meatal specimens with ZEISS, Stemi 305 Stereomicroscope

**Fig. 3.5:** Surface profiling of metal specimens with Surtronic S -128

## 3.3 Results and Discussions

### 3.3.1 Selection of PCM

For the current study (solar heating application), 87 feasible PCMs (melting temperature range 40ºC to 90ºC) are initially identified from literature review, the details of which are included in the Appendix 3A [4, 24-27]. The price of the PCMs is taken from the commercial website because the commercial grade PCM is considered for the present

study [28]. Following the pre-selection process, the numbers of candidates are drastically reduced by only considering candidates from fatty acids, polyalcohol, paraffins, non-paraffins, and fatty acids due to their consistent melting, good nucleating capabilities, minimal cost, and high heat of fusion leaving only 17 PCMs to be considered in the decision matrix. Table 3.3 displays a list of all the selected PCM candidates (shortlisted from Appendix 3A) for solar heating applications together with their thermophysical characteristics.

**Table 3.3:** Thermophysical properties of the pre-selected PCM for heating application

| S.No. | PCM | Melting temperature (ºC) | Latent heat of fusion (J/g) | Thermal conductivity (W/mK) | Density (kg/m$^3$) | Reference |
|---|---|---|---|---|---|---|
| 1 | Paraffin wax | 68 | 210 | 0.4(solid), 0.2(liquid) | 840 | [24,25] |
| 2 | Bee wax | 61.8 | 177 | 0.25 | 961 | [24] |
| 3 | Acrylic acid | 68 | 115 | 0.49 (solid) 0.51 (liquid) | 1051 | [24-26] |
| 4 | Benzylamine | 78 | 174 | n.a. | 981 | [24- 26] |
| 5 | Stearic acid | 64 | 203 | 0.29 | 847 (liquid), 965 (solid) | [4] [24-27] |
| 6 | Acetamide | 81 | 241 | 0.5 | 998 (liquid), 1159 (solid) | [4] [24-26] |
| 7 | Myristic acid | 49–58 | 186, 199 | 0.17 (solid) | 861 (liquid), 990 (solid) | [4] [24,26,27] |
| 8 | Palmatic acid | 55 - 64 | 163, 185.4 | 0.162 (liquid, 68 ºC), 0.159 (liquid, 80 ºC), | 850 (liquid, 65 ºC), 989 (solid, 24 ºC) | [4] [24-27] |
| 9 | Lauric acid | 42–44 | 178 | 0.147 (liquid, 50 ºC) | 870 (liquid, 50 ºC), 1007 (solid, 24 ºC) | [4] [24-27] |
| 10 | Phenylacetic acid | 76.7 | 102 | n.a. | 1080 | [24] |
| 11 | Hypophosphoric acid | 55 | 213 | n.a. | n.a. | [24] |
| 12 | Glycolic acid | 63 | 109 | n.a. | 1490 | [24] |
| 13 | Glycerol tristearate | 63.45 | 149.4 | n.a. | 862 | [27] |
| 14 | Napthelene | 80 | 147.7 | 0.132 (liquid), 0.341 (solid) | 976 (liquid), 1145 (solid) | [24] |
| 15 | Biphenyl | 71 | 119.2 | n.a. | 994 (liquid), 1166 (solid) | [26] |
| 16 | Pentadecanoic acid | 52–53 | 178 | n.a. | 842 | [24,27] |
| 17 | Arachidic | 74 | 227 | 0.181 | 824 | [27] |

Table 3.4 displays the values for the enthalpy of fusion, maximum operating temperature (flash point and boiling point), breadth of phase transition (melting and freezing point width), and price of the PCMs that were previously pre-screened.

**Table 3.4:** Value of the decision parameters

| S.No. | PCM | Latent heat of fusion (J/g) | Maximum operating temperature, (Flash point and Boiling point), $T_{max}$ (°C) | Width of phase change, (Melting and freezing temperature difference) (°C) | Price/kg (INR) [28] |
|---|---|---|---|---|---|
| 1 | Paraffin wax | 210 | 199, 370 | 2.8 [29] | 90 |
| 2 | Bee wax | 177 | 204.4 | 3.59 [30] | 345 |
| 3 | Acrylic acid | 115 | 50, 141.3 [31] | 0.5 [31] | 210 |
| 4 | Benzylamine | 174 | 65, 185 [32] | 0 [32] | 300 |
| 5 | Stearic acid | 203 | 196.11, 361 [33] | 2 [33] | 80 |
| 6 | Acetamide | 241 | 126, 221 [34] | 2 [34] | 300 |
| 7 | Myristic acid | 186 | 110, 326 [35] | 7.12 [36] | 190 |
| 8 | Palmatic acid | 163 | 113, 271.5 [37] | 1.5 [37] | 190 |
| 9 | Lauric acid | 178 | 160, 225 [38] | 2 [38] | 196 |
| 10 | Phenylacetic acid | 102 | 132, 265 [39] | 2 [39] | 350 |
| 11 | Hypophosphoric acid | 213 | 130 | 1 | 480 |
| 12 | Glycolic acid | 109 | 300, 169 | 5 [40] | 500 |
| 13 | Glycerol tristearate | 149.4 | 327, 260 [41] | 2 [41] | 235 |
| 14 | Napthelene | 147.7 | 80, 218 [42] | 1.5 [42] | 145 |
| 15 | Biphenyl | 119.2 | 110, 255 [43] | 2 [43] | 350 |
| 16 | Pentadecanoic acid | 178 | 110, 257 [44] | 2 [44] | 210 |
| 17 | Arachidic | 227 | 134 [45], 328 [46] | 2.6 [47] | 200 |

Table 3.5 shows the results obtained after applying the multi attribute decision matrix based on the scoring criteria shown in Table 3.1 and using the weights that correspond to Scenario A and B in Table 2 only to pre-selected PCM which seems to be the most appropriate for the solar heating application. The best three PCMs according to average score and ranking are stearic acid (51 % in scenario A, 48 % in scenario B), paraffin wax (51 % in scenario A, 48 % in scenario B) and acetamide (45 % in scenario A, 44 % in scenario B). Therefore, stearic acid, paraffin wax and acetamide will be further directed

towards thermal stability and corrosivity test for its application in solar heating applications such as solar dryer, space heating, process heating.

**Table 3.5:** Pre-selected PCM candidates overall average score and ranking

| S. No. | Scenario A | | | Scenario B | | |
|---|---|---|---|---|---|---|
| | PCM | (Average Score %) | Ranking | PCM | (Average Score %) | Ranking |
| 1 | Paraffin wax | 51 | 1 | Paraffin wax | 48 | 1 |
| 2 | Stearic acid | 51 | 1 | Stearic acid | 48 | 1 |
| 3 | Acetamide | 45 | 2 | Acetamide | 44 | 2 |
| 4 | Arachidic | 36 | 3 | Benzylamine | 36 | 3 |
| 5 | Benzylamine | 33 | 4 | Hypophosphoric acid | 36 | 3 |
| 6 | Glycerol tristearate | 33 | 4 | Glycerol tristearate | 36 | 3 |
| 7 | Hypophosphoric acid | 33 | 4 | Arachidic | 32 | 4 |
| 8 | Palmatic acid | 30 | 5 | Napthelene | 32 | 4 |
| 9 | Lauric acid | 30 | 5 | Acrylic acid | 32 | 4 |
| 10 | Pentadecanoic | 30 | 5 | Palmatic acid | 28 | 5 |
| 11 | Bee wax | 30 | 5 | Lauric acid | 28 | 5 |
| 12 | Acrylic acid | 27 | 6 | Pentadecanoic | 28 | 5 |
| 13 | Napthelene | 27 | 6 | Bee wax | 28 | 5 |
| 14 | Myristic acid | 24 | 7 | Phenylacetic acid | 24 | 6 |
| 15 | Phenylacetic acid | 24 | 7 | Biphenyl | 20 | 7 |
| 16 | Glycolic acid | 21 | 8 | Myristic acid | 12 | 7 |
| 17 | Biphenyl | 18 | 9 | Glycolic acid | 16 | 8 |

### 3.3.2 Thermal stability analysis of the selected PCMs

#### 3.3.2.1 Thermal degradation behaviour of PCM

The thermograms of the fresh (a) paraffin wax, (b) stearic acid and (c) acetamide sample are shown in Fig. 3.6. According to TGA thermograms, paraffin wax and stearic acid PCMs both degrade completely only until temperatures of 348.2 ºC and 286.9 ºC leaving less than 1 wt% of the original sample, respectively, whereas the required maximum operating temperature of PCM is considered as 120 ºC for low to medium solar heating application. Acetamide starts degrading at 110 ºC and major portion of mass (~92%) decomposes by 188 ºC remaining only 0.34% at boiling point (220.7 ºC). Thus, all the PCMs can be seen clearly sustaining 120 ºC where they degrade up to 0.31 wt% in case of paraffin wax and 0.03 wt% in case of stearic acid and acetamide can be considered appropriate for thermal storage applications up to 110 ºC without any loss of PCM

material. According to the findings of another study on acetamide and acetamide/expanded graphite composite, the initial breakdown temperatures are 122 ºC and 139 ºC, respectively, and the highest mass losses of acetamide and acetamide/expanded graphite composite occurred at 209 ºC and 208 ºC, respectively [48].

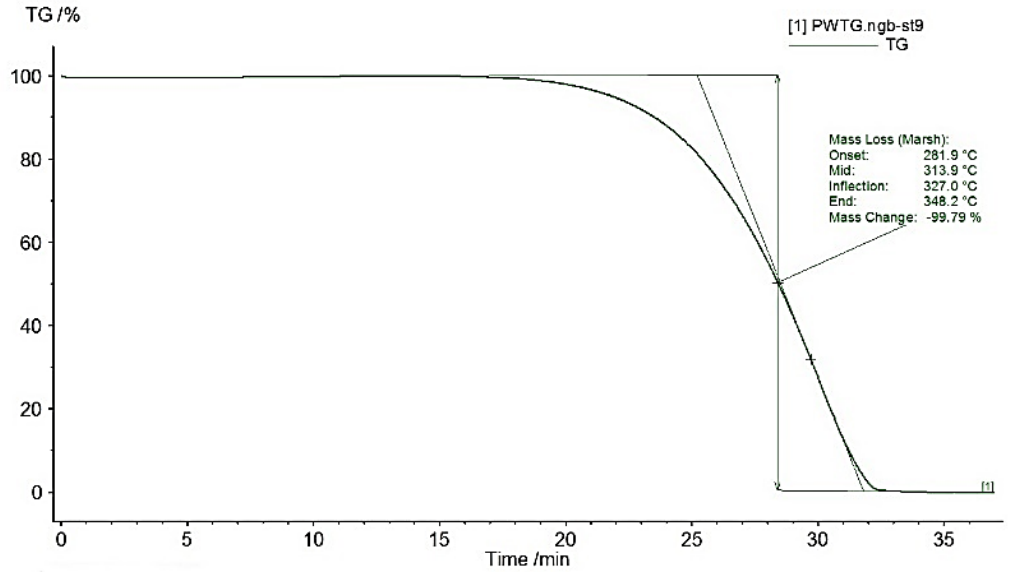


(a) paraffin wax

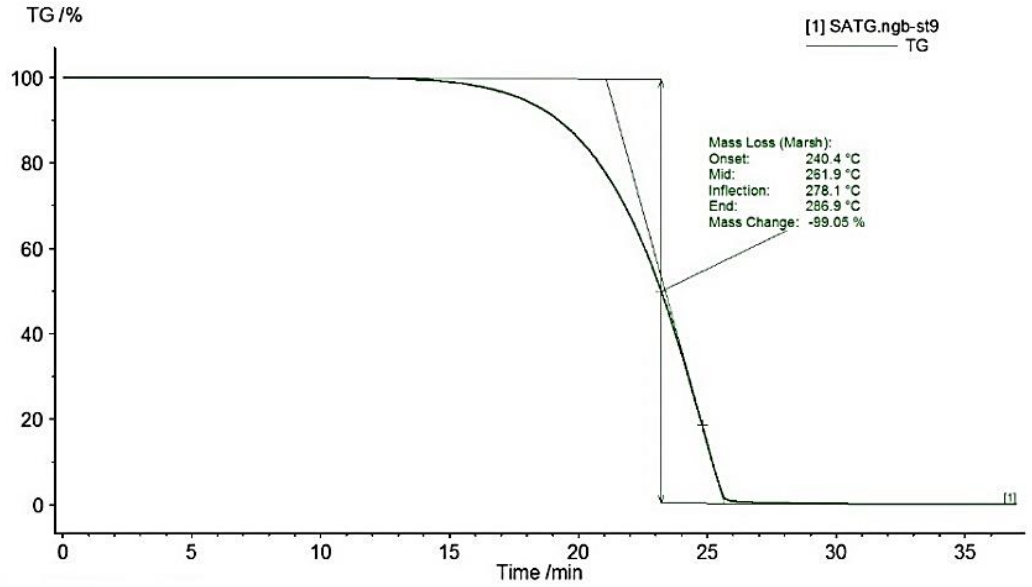


(b) stearic acid

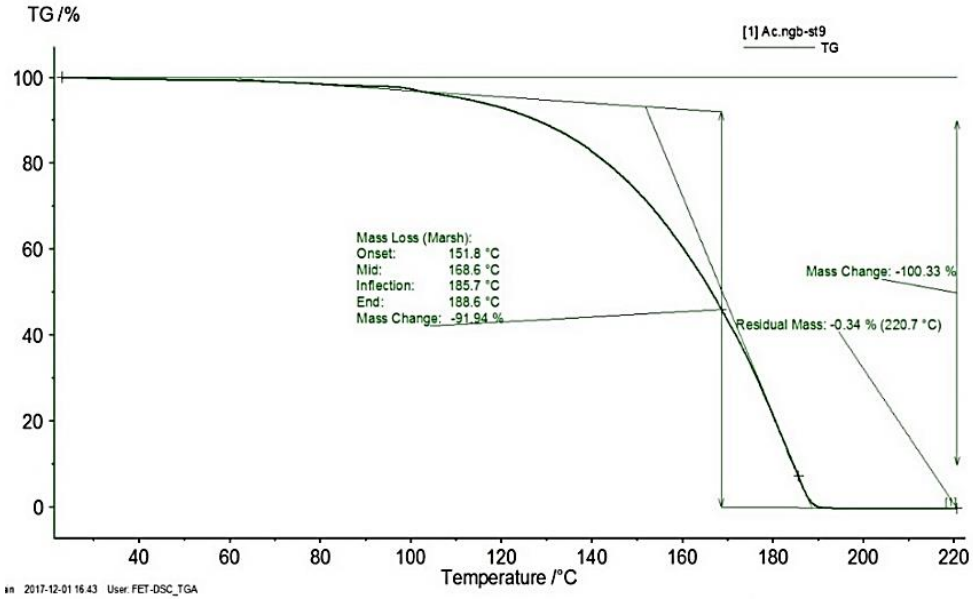


(c) acetamide

**Fig. 3.6:** TGA curve of (a) paraffin wax, (b) stearic acid, and (c) acetamide

### 3.3.2.2 Thermophysical properties of the PCM on repeated thermal cycles

Accelerated thermal cycling test is conducted to determine the thermo-physical properties of paraffin wax, stearic acid and acetamide after repeated thermal cycles up to 1000th cycle at an interval of 100 cycles. The changes in melting temperature and latent heat of fusion due to thermal cycling are investigated through DSC. Three representative DSC curve of paraffin wax, stearic acid and acetamide indicating (i) onset melting temperature, (ii) peak melting temperature, (iii) end set melting temperature and (iv) latent heat of fusion corresponding to 0th (fresh), 500th and 1000th thermal cycles are presented in Fig. 3.7, 3.8 and 3.9 respectively.

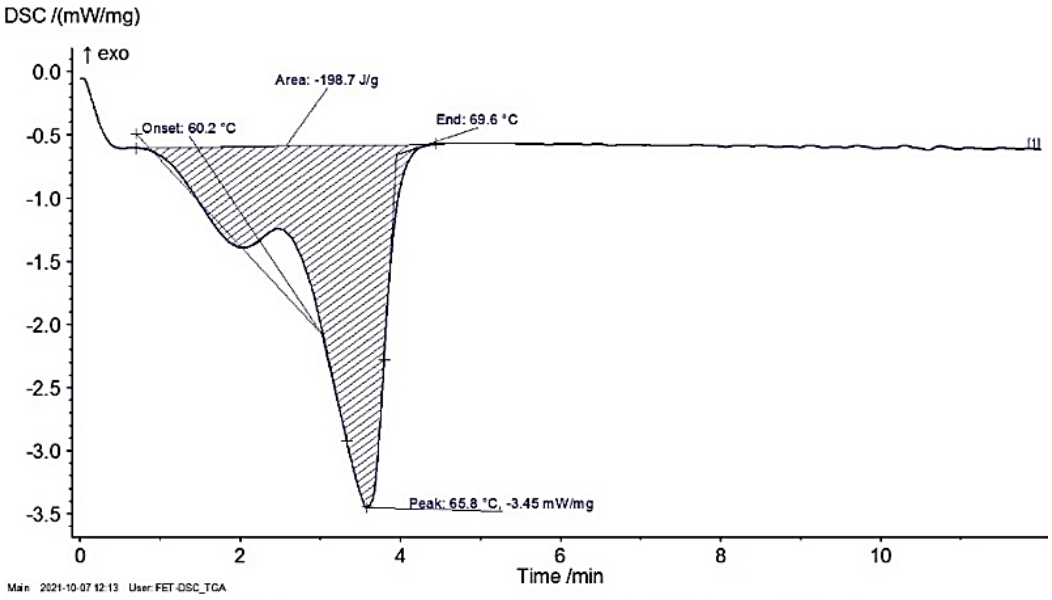
DSC /(mW/mg)
↑ exo
0.0
-0.5
-1.0
-1.5
-2.0
-2.5
-3.0
-3.5
Area: -198.7 J/g
Onset: 60.2 °C
End: 69.6 °C
[1]
Peak: 65.8 °C, -3.45 mW/mg
0
2
4
6
8
10
Time /min
Main 2021-10-07 12:13 User: FET-DSC_TGA

(a)

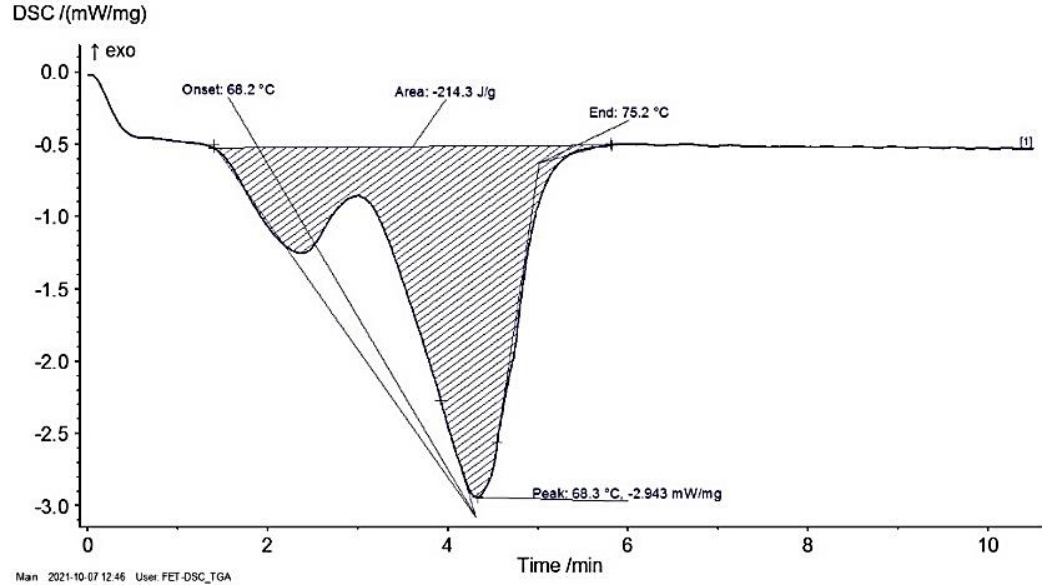
DSC /(mW/mg)
↑ exo
0.0
-0.5
-1.0
-1.5
-2.0
-2.5
-3.0
Onset: 68.2 °C
Area: -214.3 J/g
End: 75.2 °C
[1]
Peak: 68.3 °C, -2.943 mW/mg
0
2
4
6
8
10
Time /min
Main 2021-10-07 12:46 User: FET-DSC_TGA

(b)

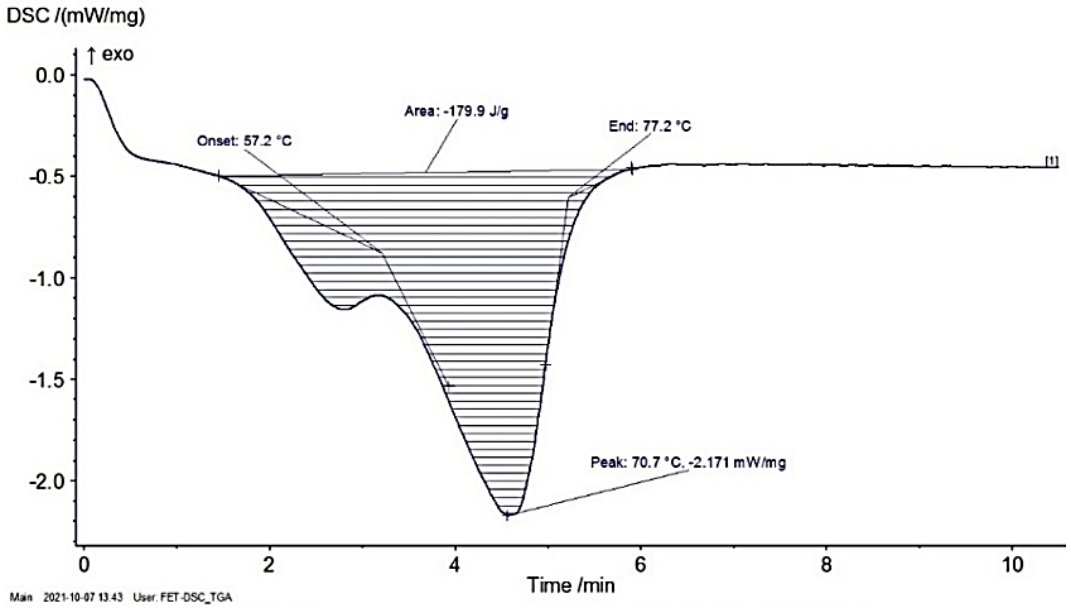


(c)

**Fig. 3.7:** DSC curve of paraffin wax at (a) $0^{th}$, (b) $500^{th}$ and (c) $1000^{th}$ thermal cycle

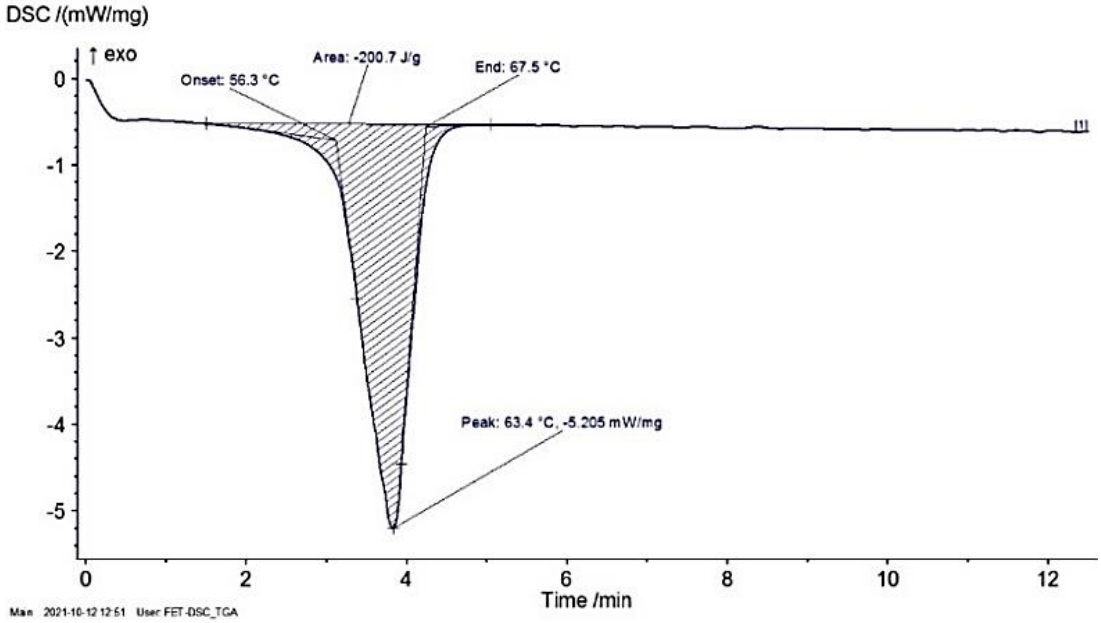


(a)

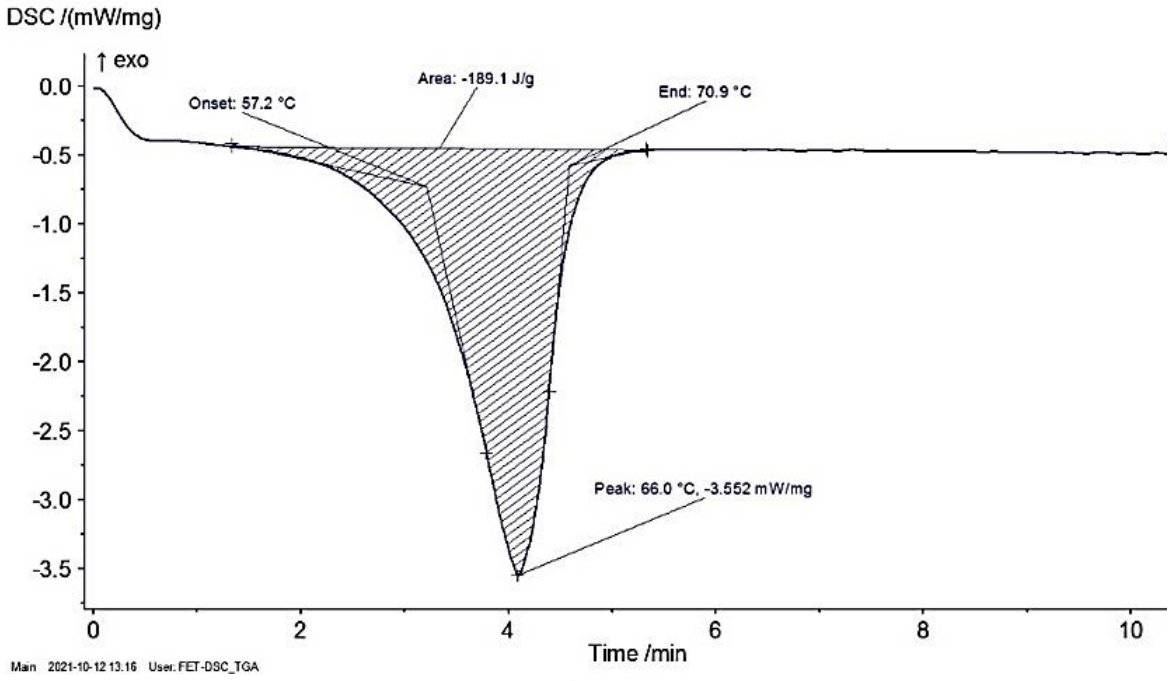


(b)

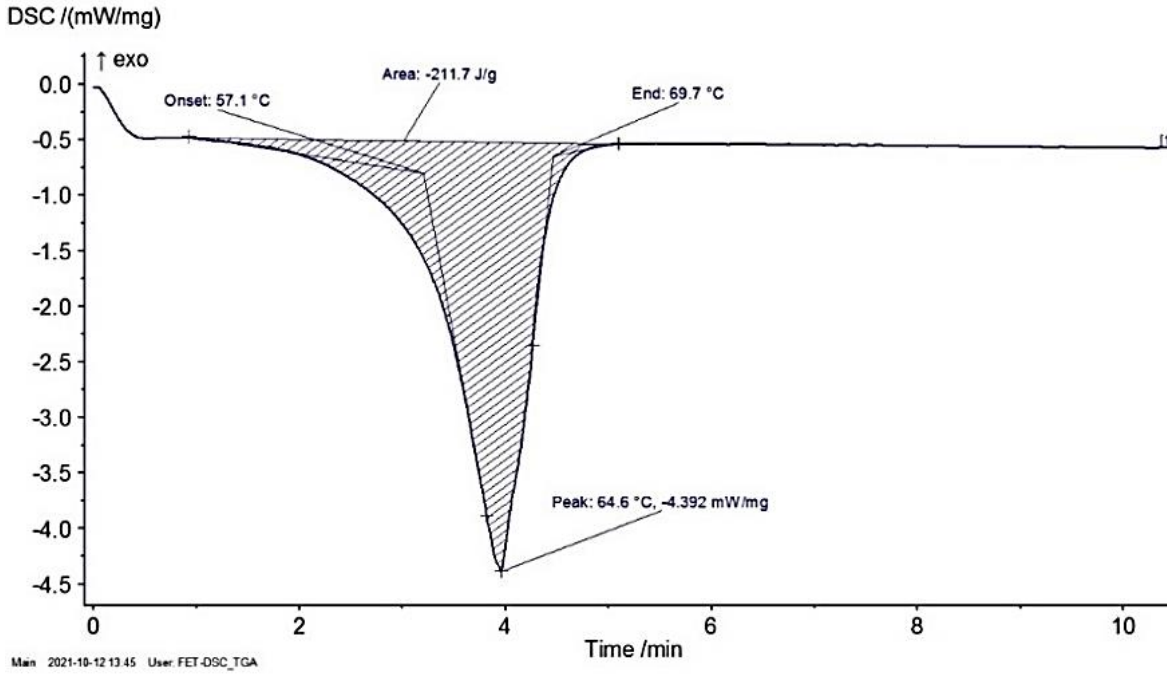


(c)

**Fig. 3.8:** DSC curve of stearic acid at (a) $0^{th}$, (b) $500^{th}$ and (c) $1000^{th}$ thermal cycle

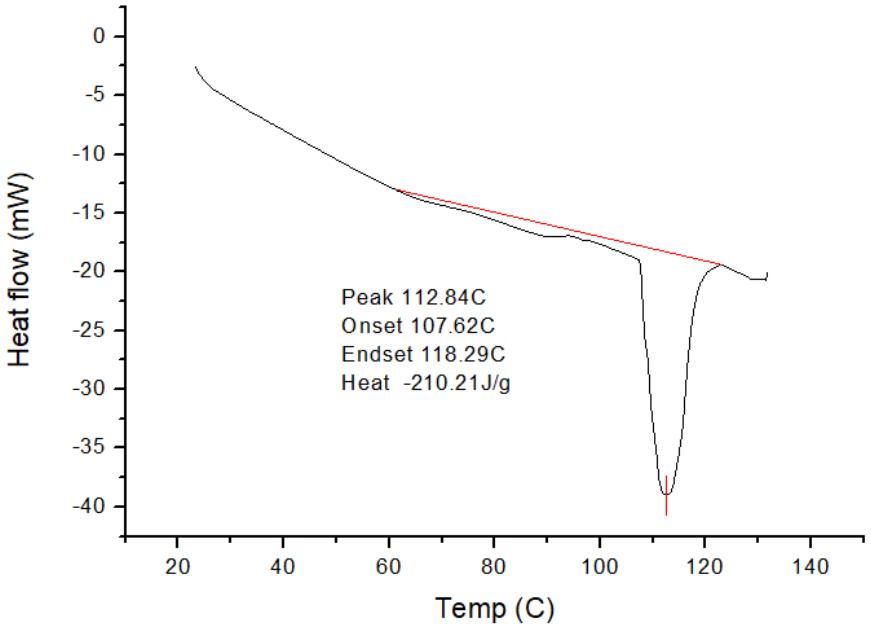
Heat flow (mW)
0
-5
-10
-15
-20
-25
-30
-35
-40
20
40
60
80
100
120
140
Temp (C)
Peak 112.84C
Onset 107.62C
Endset 118.29C
Heat -210.21J/g

(a)

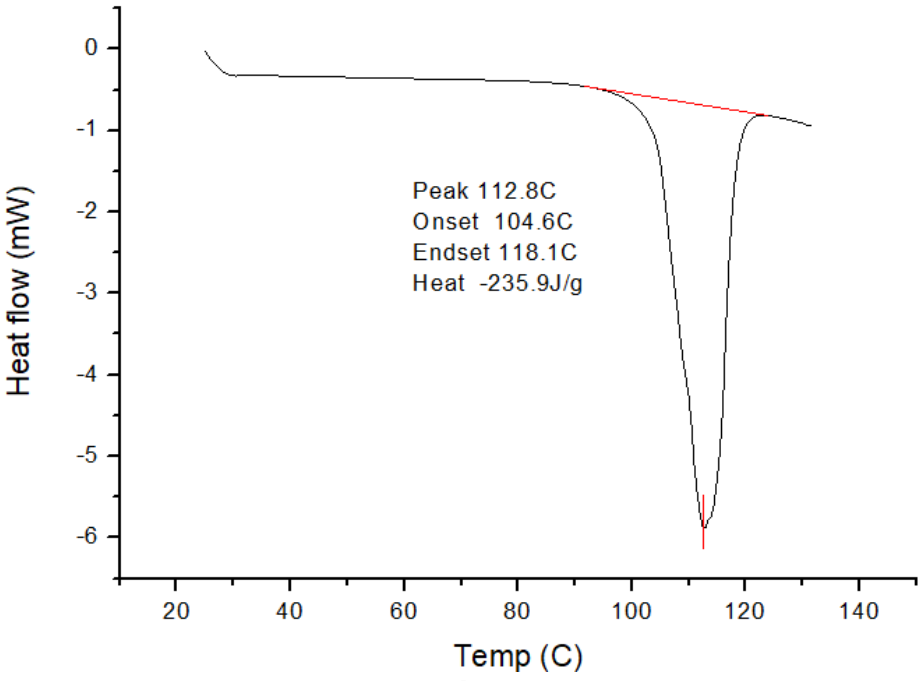
Heat flow (mW)
0
-1
-2
-3
-4
-5
-6
20
40
60
80
100
120
140
Temp (C)
Peak 112.8C
Onset 104.6C
Endset 118.1C
Heat -235.9J/g

(b)

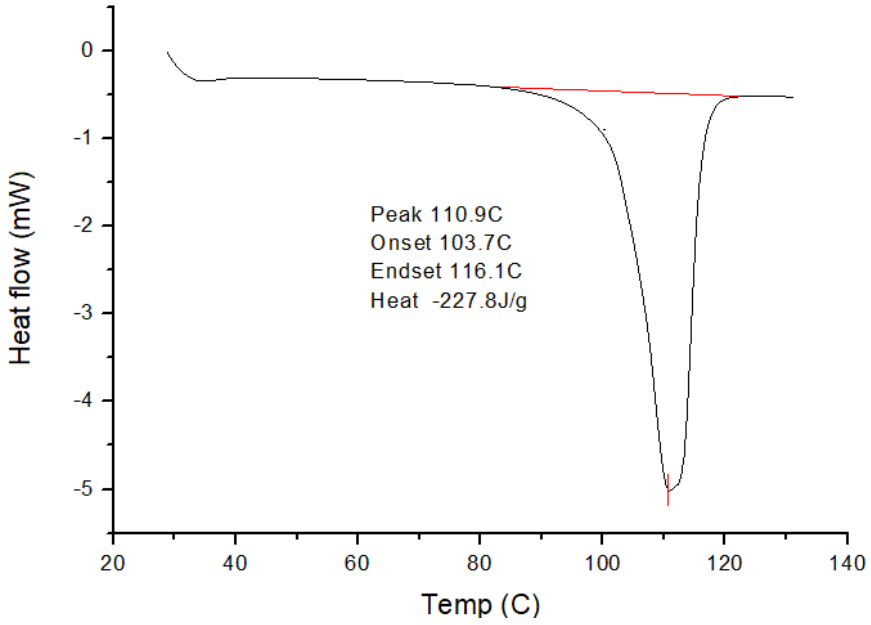


(c)

**Fig. 3.9:** DSC curves of acetamide at (a) $0^{th}$, (b) $500^{th}$ and (c) $1000^{th}$ thermal cycle

The onset melting point, peak melting point and latent heat of fusion of the selected PCM such as paraffin wax, stearic acid and acetamide from the DSC curves are represented by relative percentage difference (RPD) as shown in Table 3.6, Table 3.7, and Table 3.8 respectively. The range of the RPD of onset melting point for paraffin wax varied from -5.98% to 13.2%. The range of melting point of paraffin wax at its the peak ranged between 0.91% to 7.44%, and the range of the enthalpy of fusion of paraffin wax varied from -9.46% to 7.85% respectively. Likewise, the RPD of onset melting point of stearic acid ranged from -4.08 % to 3.19 %, peak melting point of stearic acid ranged from 0.47 % to 4.73 % and latent heat of fusion of stearic acid ranged from -5.77 % to 5.48 % respectively. Also, the RPD of onset melting point of acetamide range from -13.19 % to 0.82 %, peak melting point of acetamide ranged from -6.62 % to 2.34 % and latent heat of fusion of acetamide range from -3.81% to 12.22 % respectively. The values at the zeroth thermal cycle are used as a baseline for determining the RPD for one thousand thermal cycles [49]. In one of the previous experiments, the melting points of the samples of commercial grade acetamide, stearic acid, and paraffin wax did not degrade consistently after repeated 1500 thermal cycles. The PCM candidates acetamide and paraffin wax are considered favourable as they exhibited reasonable constancy during the cycling procedure. Nevertheless, acetamide absorbs moisture from its environment.

The changing behaviour of acetamide during thermal cycling, are attributed due to possible moisture absorption by PCM and due to its inability to form desired crystal structure after repeated thermal cycling. To minimize the effect of ambient conditions on its thermal properties, desiccator is used for intermediate storage and handling during cycling testing [50]. However, to understand the behaviour of the PCM under natural conditions, the samples are kept open during the experimentation. Effect of ambient moisture absorbed by PCM material might have modified the melting temperature as indicated by DSC results. Similar to changing melting behaviour of PCM, the changes in latent heat of fusion during thermal cycling has also been attributed to states of crystallization. For example, Emons et al. [51] examined the thermal properties of acetamide and reported to form stable and unstable compounds of acetamide during thermal cycling. Reduction of latent heat of fusion up to 50 kJ/kg of PCM is reported primarily due to presence of moisture in the sample. In addition to the crystallization behaviour of PCM, the presence of impurities also reported to contribute to the variations in latent heat and phase transition temperature. It is also reported that quality of acetamide varies between the commercial and laboratory grade [52]. Despite marginal variations of the thermal properties as reflected through the DSC results, all the three PCMs can be considered as a potential PCM for latent heat based solar dryer application due to acceptable level of RPD.

**Table 3.6:** Thermal stability of solid-liquid phase transition of paraffin wax

| S. No. | No. of cycles | Onset temperature (ºC) | RPD (%) of onset temperature | Peak temperature (ºC) | RPD (%) of peak temperature | Latent heat of fusion (J/g) | RPD (%) of latent heat of fusion |
|---|---|---|---|---|---|---|---|
| 1 | 0 | 60.2 | -- | 65.8 | -- | 198.7 | -- |
| 2 | 100 | 58 | -3.65 | 66.4 | 0.91 | 190.7 | -4.37 |
| 3 | 200 | 57.2 | -4.98 | 69 | 4.86 | 212.2 | 6.79 |
| 4 | 300 | 62.4 | 3.65 | 69.4 | 5.47 | 192.2 | -3.27 |
| 5 | 400 | 56.6 | -5.98 | 69.8 | 6.07 | 188.3 | -5.23 |
| 6 | 500 | 68.2 | 13.2 | 68.3 | 3.79 | 214.3 | 7.85 |
| 7 | 600 | 56.3 | -6.47 | 68.7 | 4.40 | 198.9 | 0.10 |
| 8 | 700 | 62.9 | 4.48 | 69.7 | 5.92 | 199.7 | 0.50 |
| 9 | 800 | 65.8 | 9.3 | 68.3 | 3.79 | 203.7 | 2.51 |
| 10 | 900 | 67.1 | 11.46 | 69.2 | 5.16 | 199.3 | 0.30 |
| 11 | 1000 | 57.2 | -4.98 | 70.7 | 7.44 | 179.9 | -9.46 |

**Table 3.7:** Thermal stability of solid-liquid phase transition of stearic acid

| S. No. | No. of cycles | Onset temperature (ºC) | RPD (%) of onset temperature | Peak temperature (ºC) | RPD (%) of peak temperature | Latent heat of fusion (J/g) | RPD (%) of latent heat of fusion |
|---|---|---|---|---|---|---|---|
| 1 | 0 | 56.3 | -- | 63.4 | -- | 200.7 | -- |
| 2 | 100 | 58.1 | 3.19 | 65.4 | 3.15 | 208 | 3.63 |
| 3 | 200 | 57.1 | 1.42 | 65.7 | 3.62 | 207.8 | 3.53 |
| 4 | 300 | 58 | 3.01 | 66.4 | 4.73 | 192.8 | -3.93 |
| 5 | 400 | 57 | 1.24 | 65.8 | 3.78 | 205.9 | 2.52 |
| 6 | 500 | 57.2 | 1.59 | 66 | 4.10 | 189.1 | -5.77 |
| 7 | 600 | 56.6 | 0.53 | 65 | 2.52 | 198.3 | -1.19 |
| 8 | 700 | 56.8 | 0.88 | 63.7 | 0.47 | 198.6 | -1.04 |
| 9 | 800 | 56.8 | 0.88 | 64.1 | 1.10 | 208.9 | 4.08 |
| 10 | 900 | 54 | -4.08 | 63.9 | 0.78 | 203.8 | 1.54 |
| 11 | 1000 | 57.1 | 1.42 | 64.6 | 1.89 | 211.7 | 5.48 |

**Table 3.8:** Thermal stability of solid-liquid phase transition of acetamide

| S. No. | No. of cycles | Onset temperature (°C) | RPD (%) of onset temperature | Peak temperature (°C) | RPD (%) of peak temperature | Latent heat of fusion (J/g) | RPD (%) of latent heat of fusion |
|---|---|---|---|---|---|---|---|
| 1 | 0 | 107.62 | -- | 112.84 | -- | 210.21 | -- |
| 2 | 100 | 108.51 | 0.82 | 114.37 | 1.35 | 215.16 | 2.35 |
| 3 | 200 | 99.89 | -7.18 | 110.28 | -2.26 | 212.48 | 1.07 |
| 4 | 300 | 94.56 | -12.13 | 105.36 | -6.62 | 203.92 | -2.99 |
| 5 | 400 | 97.47 | -9.43 | 106.41 | -5.69 | 207.54 | -1.27 |
| 6 | 500 | 104.60 | -2.80 | 112.8 | -0.03 | 235.9 | 12.22 |
| 7 | 600 | 106.37 | -1.16 | 115.49 | 2.34 | 217.34 | 3.39 |
| 8 | 700 | 102.30 | -4.94 | 113.45 | 0.54 | 212.31 | 0.99 |
| 9 | 800 | 98.75 | -8.24 | 107.96 | -4.32 | 202.20 | -3.81 |
| 10 | 900 | 93.42 | -13.19 | 105.62 | -6.39 | 206.58 | -1.72 |
| 11 | 1000 | 103.70 | -3.64 | 110.90 | -1.71 | 227.80 | 8.36 |

### 3.3.3 Compatibility study of PCM

#### 3.3.3.1 Corrosion study

Corrosion test is carried out to study the compatibility of the built materials of the thermal storage container such as aluminium, copper, stainless steel, and mild steel with the selected PCMs viz., stearic acid, paraffin wax and acetamide. Table 3.9 shows the results of a corrosion investigation in which metal specimens or samples were immersed in PCMs and subjected to 1000 heating and cooling thermal cycles, that are indicated by corrosion rate. The results of the corrosion study clearly show that with all the PCMs the corrosion rate of copper is highest followed by mild steel, aluminium, and stainless steel. With reference to the corrosion rate analysis that are used in industry as tabulated in Table 3.10 [53,54] and the corrosion rate of the present study as tabulated in Table 3.9, we can conclude that compatibility of all the PCMs with aluminium, copper and mild steel are recommended for long term storage. Stainless steel is highly recommended for long term storage but owing to its high price finally we can consider aluminium as most preferable container material for latent heat based solar dryer with stearic acid, paraffin wax and acetamide.

**Table 3.9:** Corrosion rate of PCM metal containers

| PCMs | Surface roughness parameters | Metal strip materials | | | |
|---|---|---|---|---|---|
| | | Aluminium | Copper | Stainless Steel | Mild Steel |
| Stearic acid | Initial mass (g) | 8.41 | 33.97 | 2.67 | 28.87 |
| | Final mass (g) | 8.36 | 33.44 | 2.66 | 28.59 |
| | Percentage of mass loss (%) | 0.55 | 2.22 | 0.52 | 0.97 |
| | Corrosion rate | 0.34 | 3.96 | 0.11 | 2.26 |
| Paraffin wax | Initial mass (g) | 8.60 | 34.44 | 2.67 | 29.33 |
| | Final mass (g) | 8.57 | 34.10 | 2.66 | 29.19 |
| | Percentage of mass loss (%) | 0.30 | 1.40 | 0.19 | 0.46 |
| | Corrosion rate | 0.19 | 2.54 | 0.04 | 1.09 |
| Acetamide | Initial mass (g) | 0.76 | 1.11 | 6.72 | 3.65 |
| | Final mass (g) | 0.75 | 1.04 | 6.71 | 3.59 |
| | Percentage of mass loss (%) | 0.98 | 6.32 | 0.08 | 1.57 |
| | Corrosion rate | 1.35 | 12.27 | 0.90 | 9.96 |

**Table 3.10:** Reference for corrosion rate analysis used in industry [53, 54]

| Corrosion rate (mg/cm$^2$ year) | Recommendation |
|---|---|
| >1000 | Destroyed within days |
| 100–999 | Not recommended for service greater than a month |
| 50–99 | Not recommended for service greater than one year |
| 10–49 | Caution recommended, based on the specific application |
| 0.3–9.9 | Recommended for long term service |
| <0.2 | Highly Recommended for long term service |

### 3.3.3.2 Surface degradation imaging of the metal samples

The morphologies of the surface of the pristine metal specimens under investigation (Stainless steel, Aluminium, mild steel, and copper) before and after treatment with stearic acid, paraffin wax, and acetamide are captured using an optical microscope (ZEISS, Stemi 305 Stereomicroscope) and are shown in Fig. 3.10 (a-h), Fig. 3.11 (a-h), and Fig. 3.12 (a-h), respectively. In comparison to the pristine samples before and after PCM treatment, the degrading effect of all components (stearic acid, paraffin wax, and acetamide) is clearly visible with cracks and pittings as shown in Figs. 3.10, 3.11, and 3.12. The micrographs for all PCMs show a higher degree of degradation for copper and mild steel surfaces compared to stainless steel and aluminium, which is attributable to the higher corrosion rate for copper and mild steel specimens as confirmed by surface profile measurement.

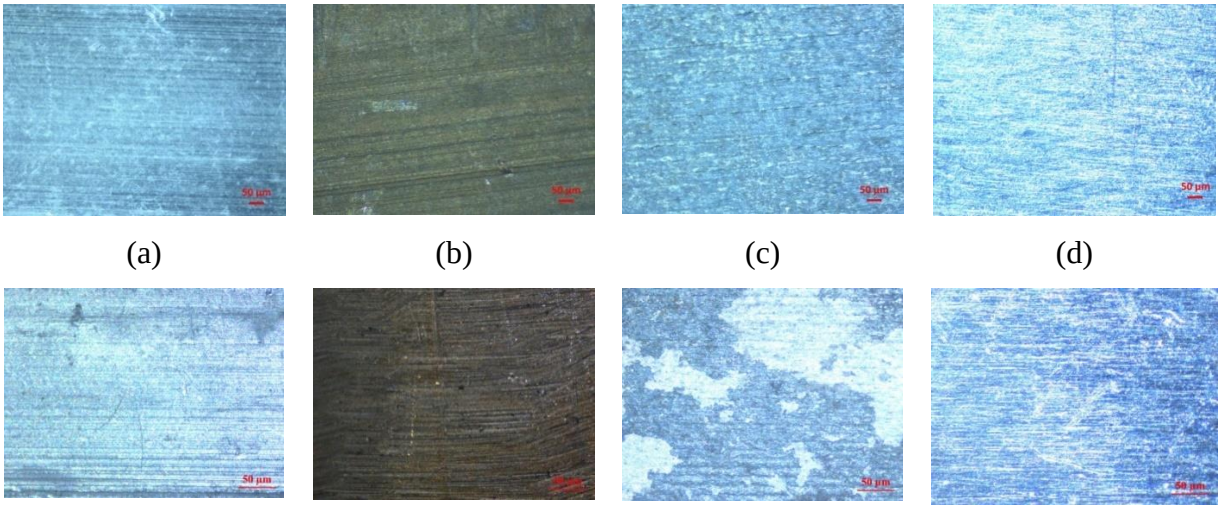

(a) (b) (c) (d)

(e) (f) (g) (h)

**Fig 3.10:** Optical micrograph of (a) aluminium, (b) copper, (c) mild Steel, and (d) stainless steel before treatment and (e) aluminium, (f) copper, (g) mild Steel, and (h) stainless steel after treatment with stearic acid

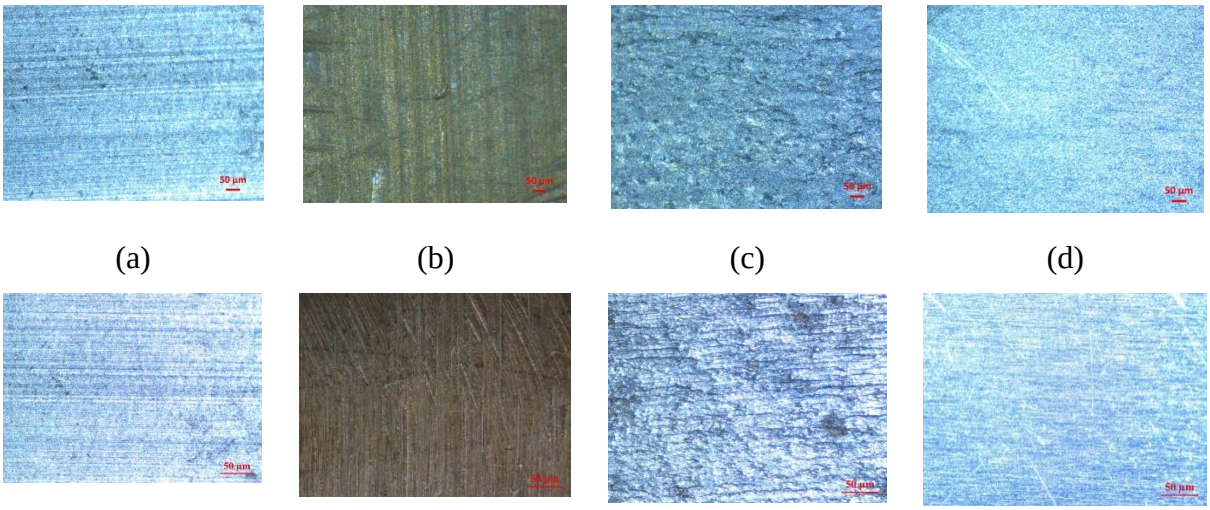

(a) (b) (c) (d)

(e) (f) (g) (h)

**Fig. 3.11:** Optical micrograph of (a) aluminium, (b) copper, (c) mild Steel, and (d) stainless steel before treatment and (e) aluminium, (f) copper, (g) mild Steel, and (h) stainless steel after treatment with paraffin wax

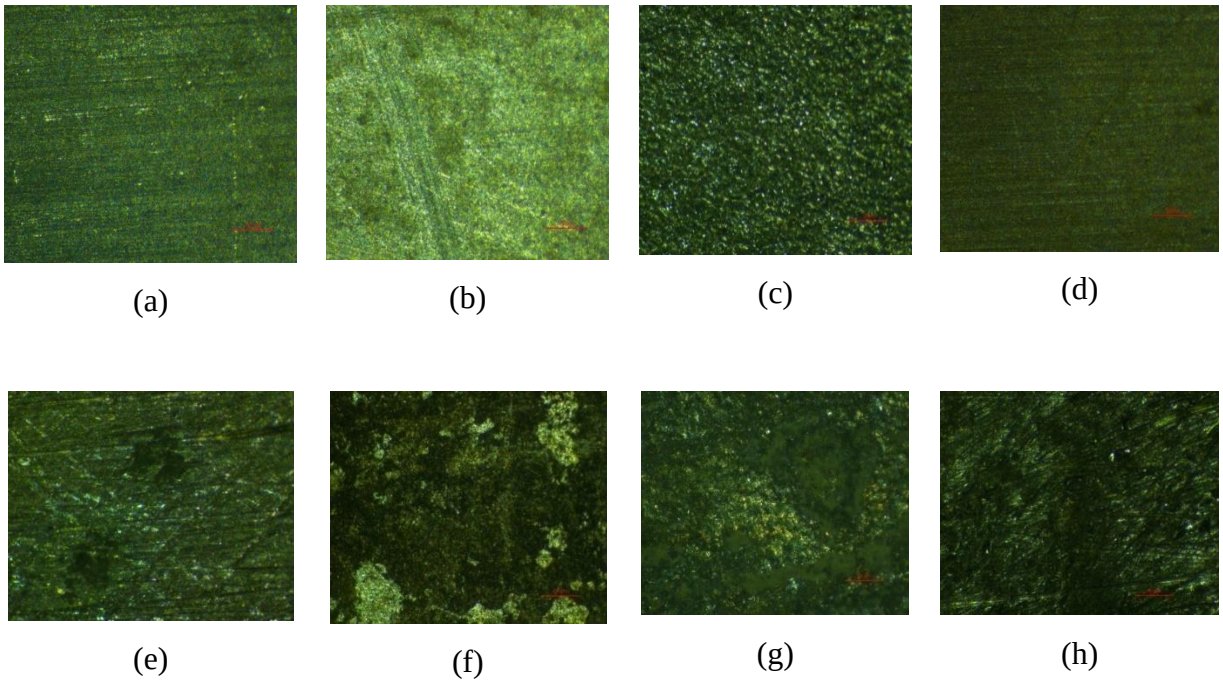


**Fig. 3.12:** Optical micrograph of (a) aluminium, (b) copper (c) mild steel (d) stainless steel (SS304) before treatment and (e) aluminium, (f) copper (g) mild steel (h) stainless steel (SS304) after treatment with acetamide

#### 3.3.3.3 Surface roughness profiling of the metal samples

Fig. 3.13, 3.14 and 3.15 depicts the surface profile measurement using a surface profilometer (Surtronic S-128) of four different metal specimens (Stainless steel, Aluminium, mild steel, and copper) before and after treatment with stearic acid, paraffin wax and acetamide respectively. It is evident from the results that the average surface roughness (Ra) as well as the maximum peak-to-valley ($P_t$) height is increased for all the samples after the treatment with PCMs. Stearic acid with highest average surface roughness and peak-to-valley height for copper to be 2.07 µm and 15.3 µm, respectively. It is followed by mild steel (0.924 µm, 7.03 µm), aluminium (0.626 µm, 4.76 µm) and stainless steel (0.149 µm, 1.26 µm) as summarized in Table 3.11. Similarly, the specimens treated with paraffin wax exhibit the highest average surface roughness and maximum peak-to-valley heights for copper (1.76 µm, 12.7 µm), followed by mild steel (0.947 µm, 6.04 µm), aluminium (0.618 µm, 5.06 µm), and stainless steel (0.162 µm, 1.12 µm). Likewise, specimens treated with acetamide exhibit the highest average surface roughness and peak-to-valley height with copper (6.31 µm and 31 µm) followed by mild steel (3.69 µm and 13.5 µm), aluminium (3.02 µm and 13 µm) and stainless steel

(2.22 µm and 9.0 µm). The results are in conformity with the corrosion tests results obtained using gravimetric analysis and are also supported by micrographs Fig. 3.10, 3.11 and 3.12.

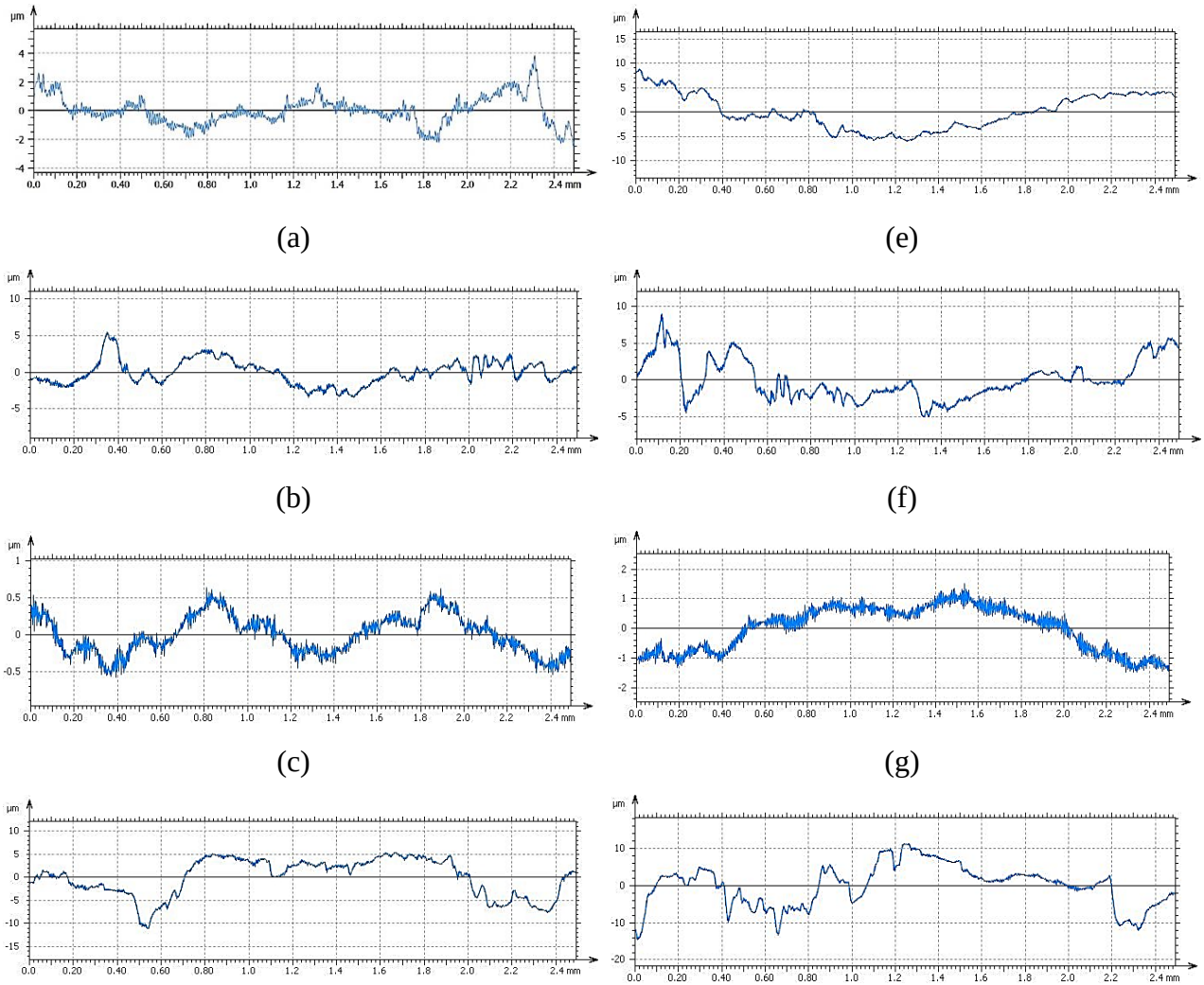


**Fig. 3.13:** Surface roughness profile of (a) aluminium, (b) mild steel, (c) stainless steel and (d) copper before treatment with stearic acid and (e) aluminium, (f) mild steel, (g) stainless steel and (h) copper after treatment with stearic acid

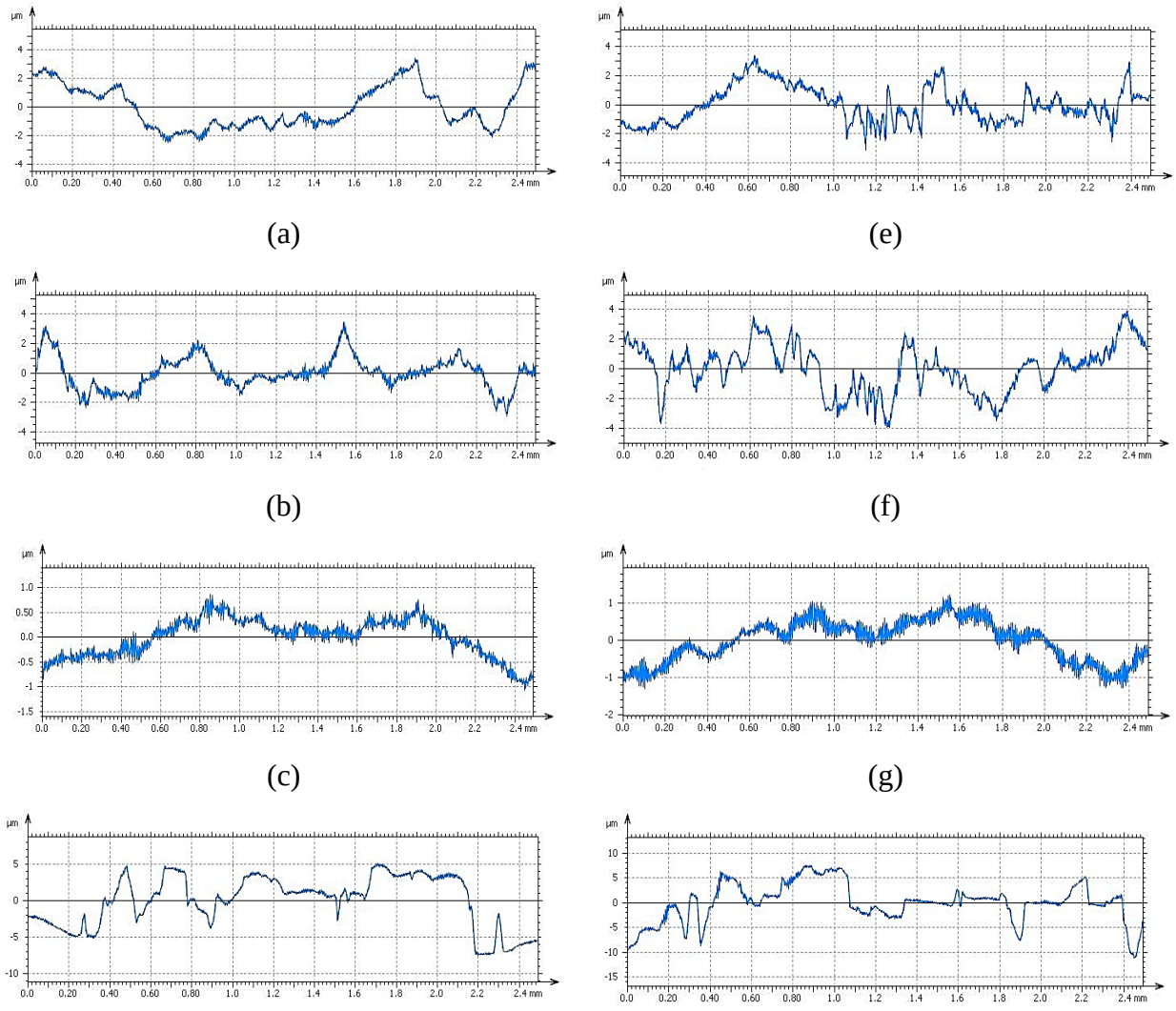


**Fig. 3.14:** Surface roughness profile of (a) aluminium, (b) mild steel, (c) stainless steel and (d) copper before treatment with paraffin wax and (e) aluminium, (f) mild steel, (g) stainless steel and (h) copper after treatment with paraffin wax

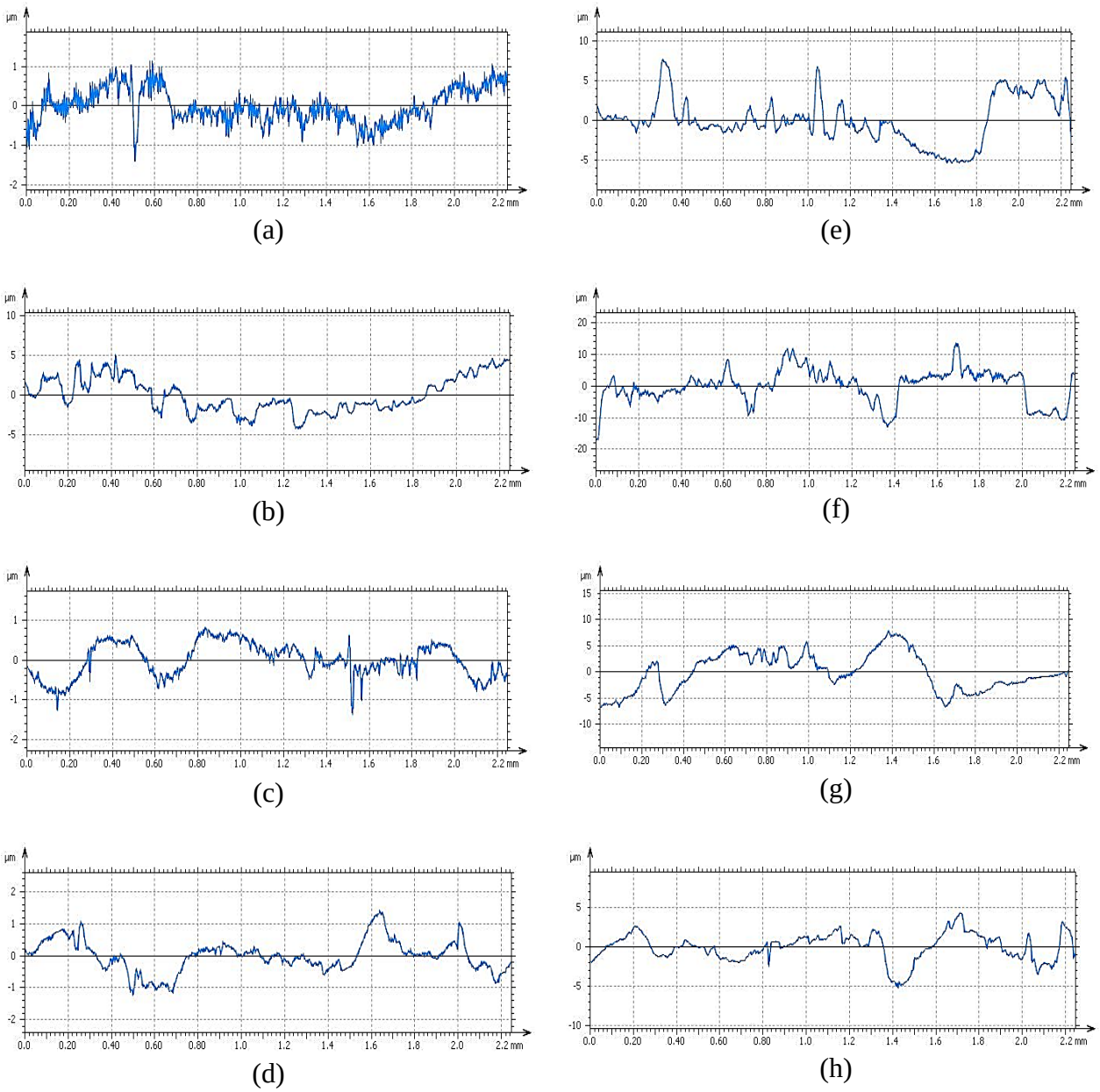


**Fig. 3.15:** Surface roughness profile of (a) aluminium, (b) copper (c) mild steel (d) Stainless steel (SS304) before treatment and (e) aluminium, (f) copper (g) mild steel (h) Stainless steel (SS304) after treatment with acetamide

**Table 3.11:** Surface profile measurement of the metal specimens before and after treatment with stearic acid paraffin wax, and acetamide

| PCMs | Surface roughness parameters | Metal strip materials | | | |
|---|---|---|---|---|---|
| | | Aluminium | Mild | Stainless | Copper |

| | | | | Steel | Steel | |
|---|---|---|---|---|---|---|
| Stearic acid | Roughness average (Ra) ($\mu$m) | Before treatment | 0.39 | 0.70 | 0.11 | 1.42 |
| | | After treatment | 0.63 | 0.92 | 0.15 | 2.07 |
| | Maximum peak-to-valley height (Rt) ($\mu$m) | Before treatment | 3.32 | 5.12 | 0.87 | 10.50 |
| | | After treatment | 4.76 | 7.03 | 1.26 | 15.30 |
| Paraffin wax | Roughness average (Ra) ($\mu$m) | Before treatment | 0.46 | 0.48 | 0.11 | 1.36 |
| | | After treatment | 0.62 | 0.95 | 0.16 | 1.76 |
| | Maximum peak-to-valley height (Rt) ($\mu$m) | Before treatment | 3.61 | 4.20 | 0.85 | 9.37 |
| | | After treatment | 5.06 | 6.04 | 1.12 | 12.70 |
| Acetamide | Roughness average (Ra) ($\mu$m) | Before treatment | 0.55 | 0.48 | 0.42 | 2.24 |
| | | After treatment | 3.02 | 3.69 | 2.22 | 6.31 |
| | Maximum peak-to-valley height (Rt) ($\mu$m) | Before treatment | 2.5 | 2.0 | 2.6 | 9.0 |
| | | After treatment | 13.0 | 13.5 | 9.0 | 31.0 |

## 3.4 Summary

The work in this Chapter presented different steps that are followed to identify and select PCMs for solar heating application of medium temperature ranging from 40-90 ºC. 17 PCMs are initially listed out of 87 PCMs available in the literatures excluding PCMs which are toxic, high price, poor thermophysical properties and corrosive. In the selection process multi attributed decision matrix is utilised that considered the melting enthalpy and temperature range, availability, cost, and maximum permitted working temperature to evaluate the potential of the most promising PCM candidates for solar heating or drying application. The best three PCMs according to average score and ranking are stearic acid (51 % in scenario A, 48 % in scenario B), paraffin wax (51 % in scenario A, 48 % in scenario B) and acetamide (45 % in scenario A, 44 % in scenario B).

The selected PCM stearic acid, paraffin wax and acetamide are further tested for thermal stability through TGA and DSC. The TGA result suggest that paraffin wax and stearic acid PCMs both degrade completely until temperatures of 348.2 ºC and 286.9 ºC. Acetamide starts degrading at 110 ºC and major portion of mass (~92%) decomposes by 188 ºC. The PCMs (paraffin wax, stearic acid and acetamide) that experienced 1000 thermal cycles are tested for DSC at every $100^{th}$ cycle to study the stability of some thermophysical properties like the onset melting point, peak melting point and latent heat of the selected PCMs. The variations of the values of onset, peak melting point and latent heat of paraffin wax, stearic acid and acetamide on repeated thermal cycles indicated by RPD % are found to be within the acceptable range and has good potential for solar heating or drying applications. The compatibility study of common metal samples with all the PCMs by corrosion test suggest that the corrosion rate of copper is highest followed by mild steel, aluminium, and stainless steel. While comparing the corrosion rate analysis that are used in industry and the corrosion rate of the present study, the compatibility of stearic acid and paraffin wax with aluminium, copper and mild steel are recommended for long term storage and stainless steel is highly recommended for long term storage but owing to its high price finally we can consider aluminium as most compatible container material for LHTES with all the PCMs. From the metal surface microscopic imaging also, it is clear that the metal specimens treated with stearic acid, paraffin wax and acetamide for 1000 thermal cycling underwent surface deformations like crack and pitting mostly seen in copper and mild steel also from the surface profile measurement it is confirmed that the copper has the highest average surface roughness and maximum peak-to-valley heights followed by mild steel, aluminium, and stainless steel. Therefore, it is recommendable for the PCMs paraffin wax, stearic acid and acetamide that aluminium and stainless steel are both compatible for LHTES application. The selected PCMs (paraffin wax, stearic acid and acetamide) and the aluminium metal container are further used for design and development of PCM based SAH in the subsequent Chapter.

**References**

[1] Huang, J., Luo, Y., Weng, M., Yu, J., Sun, L., Zeng, H., ... & Guo, Z. Advances and applications of phase change materials (PCMs) and PCMs-based

technologies. *ES Materials & Manufacturing*, 13: 23-39, 2021.

[2] Weiss, L., & Jha, R. Small-Scale Phase Change Materials in Low-Temperature Applications: A Review. *Energies*, 16(6):2841, 2023.

[3] Socaciu, L. G. Thermal energy storage with phase change material. *Leonardo Electronic Journal of Practices and Technologies*, 20: 75-98. 2012.

[4] Abhat, A. Low temperature latent heat thermal energy storage: heat storage materials. *Solar energy*, 30(4):313-332,1983.

[5] Mettawee, E. B. S., & Assassa, G. M. Thermal conductivity enhancement in a latent heat storage system. *Solar energy*, 81(7):839-845, 2007.

[6] Chiu, J. N. Heat transfer aspects of using phase change material in thermal energy storage applications. PhD thesis, School of Industrial Engineering and Management, KTH Royal Institute of Technology, 2011.

[7] Vasu, A., Hagos, F. Y., Noor, M. M., Mamat, R., Azmi, W. H., Abdullah, A. A., & Ibrahim, T. K. Corrosion effect of phase change materials in solar thermal energy storage application. *Renewable and Sustainable Energy Reviews*, 76:19-33, 2017.

[8] S. Kuravi, J. Trahan, D. Y. Goswami, M. M. Rahman, & E. K. Stefanakos, Thermal energy storage technologies and systems for concentrating solar power plants. *Progress in Energy and Combustion Science*, 39:285-319, 2013.

[9] M. Liu, J. C. Gomez, C. S. Turchi, N. H. S. Tay, W. Saman, & F. Bruno, Determination of thermo-physical properties and stability testing of high-temperature phase-change materials for CSP applications. *Solar Energy Materials and Solar Cells*, 139:81-87, 2015.

[10] Gomez, J., Glatzmaier, G. C., Starace, A., Turchi, C., & Ortega, J. High temperature phase change materials for thermal energy storage applications (No. NREL/CP-5500-52390). National Renewable Energy Lab. (NREL), Golden, CO (United States), 2011.

[11] Devanuri, J. K., Gaddala, U. M., & Kumar, V. Investigation on compatibility and thermal reliability of phase change materials for low-temperature thermal energy storage. *Materials for Renewable and Sustainable Energy*, 9:1-16, 2020.

[12] Miró, L., Barreneche, C., Ferrer, G., Solé, A., Martorell, I., & Cabeza, L. F. Health hazard, cycling and thermal stability as key parameters when selecting a suitable phase change material (PCM). *Thermochimica acta*, 627:39-47, 2016.

[13] Vasu, A., Hagos, F. Y., Noor, M. M., Mamat, R., Azmi, W. H., Abdullah, A. A., & Ibrahim, T. K. Corrosion effect of phase change materials in solar thermal energy storage application. *Renewable and Sustainable Energy Reviews*, 76:19-33, 2017.

[14] Jaya Krishna, D., & Kochar, S. The metallographic study of corrosion of metals with latent heat storage materials suitable for solar hot water system. *Transactions of the Indian Ceramic Society*, 76(2):133-141, 2017.

[15] Sharma, V. K., Colangelo, A., & Spagna, G. Experimental performance of an indirect type solar fruit and vegetable dryer. *Energy conversion and management*, 34(4):293-308, 1993.

[16] Genc, M., Inci, B., Genc, Z. K., AKSU CANBAY, C. A. N. A. N., & Sekerci, M. Preparation and investigations of thermal properties of copper oxide, aluminium oxide and graphite based on new organic phase change material for thermal energy storage. *Bulletin of Materials Science*, 38:343-350, 2015.

[17] Yu, S., Jeong, S. G., Chung, O., & Kim, S. Bio-based PCM/carbon nanomaterials composites with enhanced thermal conductivity. *Solar Energy Materials and Solar Cells*, 120:549-554, 2014.

[18] Jeong, S. G., Jeon, J., Cha, J., Kim, J., & Kim, S. Preparation and evaluation of thermal enhanced silica fume by incorporating organic PCM, for application to concrete. *Energy and Buildings*, 62:190-195, 2013.

[19] Alkan, C., Kaya, K., & Sarı, A. Preparation and thermal properties of ethylene glycole distearate as a novel phase change material for energy storage. *Materials Letters*, 62(6-7):1122-1125, 2008.

[20] Jeong, S. G., Jeon, J., Lee, J. H., & Kim, S. Optimal preparation of PCM/diatomite composites for enhancing thermal properties. *International Journal of Heat and Mass Transfer*, 62:711-717, 2013.

[21] El-Sebaii, A. A., & Al-Agel, F. Fast thermal cycling of acetanilide as a storage material for solar energy applications. *Journal of solar energy engineering*, 135(2), 2013.

[22] El-Sebaii, A. A., Al-Heniti, S., Al-Agel, F., Al-Ghamdi, A. A., & Al-Marzouki, F. One thousand thermal cycles of magnesium chloride hexahydrate as a promising PCM for indoor solar cooking. *Energy Conversion and Management*, 52(4):1771-1777, 2011.

[23] Moreno, P., Miró, L., Solé, A., Barreneche, C., Solé, C., Martorell, I., & Cabeza, L. F. Corrosion of metal and metal alloy containers in contact with phase change materials (PCM) for potential heating and cooling applications. *Applied Energy*, 125:238-245, 2014.

[24] Sharma, A., Tyagi, V. V., Chen, C. R., & Buddhi, D. Review on thermal energy storage with phase change materials and applications. *Renewable and Sustainable energy reviews*, 13(2):318-345, 2009.

[25] Da Cunha, J. P., & Eames, P. Thermal energy storage for low and medium temperature applications using phase change materials–a review. *Applied energy*, 177:227-238, 2016.

[26] Zalba, B., Marın, J. M., Cabeza, L. F., & Mehling, H. Review on thermal energy storage with phase change: materials, heat transfer analysis and applications. *Applied thermal engineering*, 23(3):251-283, 2003.

[27] Sarier, N., & Onder, E. Organic phase change materials and their textile applications: an overview. *Thermochimica acta*, 540: 7-60, 2012.

[28] India MART. https://my.indiamart.com/. (Accessed on 21/02/2023).

[29] Qin, Z., Dubey, S., Choo, F. H., Deng, H., & Duan, F. Low-grade heat collection from a latent heat thermal energy storage unit. In *15th IEEE Intersociety Conference on Thermal and Thermomechanical Phenomena in Electronic Systems (ITherm)*, pages 1248-1254, 2016 May. IEEE.

[30] Rawi, S., Amin, M., Kusrini, E., & Putra, N. Characterization of shape-stabilized phase change material using beeswax and functionalized multi-walled carbon nanotubes. In *IOP conference series: earth and environmental science*, Volume 105, No. 1, page 012042, 2018. IOP Publishing.

[31] National Center for Biotechnology Information. PubChem Compound Summary for CID 6581, Acrylic acid. https://shorturl.at/adT18. (Accessed on 23/11/2022).

[32] Sigma-Aldrich, Safety data sheet, Bezylamine. https://shorturl.at/epsvY. (Accessed on 23/11/2022).

[33] ThermoFisher SCIENTIFIC, Safety data sheet, Stearic acid. https://shorturl.at/cloHU. (Accessed on 23/11/2022).

[34] Sigma-Aldrich, Safety data sheet, Acetamide. https://shorturl.at/hmyOU. (Accessed on 23/11/2022).

[35] ThermoFisher SCIENTIFIC, Safety data sheet, Myristic acid. https://shorturl.at/bzGQT. (Accessed on 23/11/2022).

[36] Harikrishnan, S., Dhass, A. D., Oztop, H. F., & Abu-Hamdeh, N. Measurement of thermophysical properties with nanomaterials on the Melting/Freezing characteristics of phase change material. *Measurement*, 199: 111477, 2022.

[37] Sigma-Aldrich, Safety data sheet, Palmitic acid. https://shorturl.at/fwW29. (Accessed on 23/11/2022).

[38] Acme-Hardesty: Sustainable Bio-Based Ingredients Supply, Lauric acid. https://shorturl.at/cnrLQ. (Accessed on 23/11/2022).

[39] Sigma-Aldrich, Safety data sheet, Phenylacetic acid. https://shorturl.at/kryDZ. (Accessed on 23/11/2022).

[40] Sigma-Aldrich, Safety data sheet, Glycolic acid. https://shorturl.at/ehHZ2. (Accessed on 23/11/2022).

[41] AK Scientific, Inc. Safety Data Sheet, Glycerol tristearate. https://shorturl.at/morQY. (Accessed on 23/11/2022).

[42] CDH fine Chemical, Material safety data sheet, Naphthalene. https://shorturl.at/bmnX8. (Accessed on 23/11/2022).

[43] Sigma-Aldrich, Safety data sheet, Biphenyl. https://shorturl.at/gmwCZ. (Accessed on 23/11/2022).

[44] Cayman Chemicals, Safety data sheet, Pentadecanoic acid. https://shorturl.at/jnGL8. (Accessed on 23/11/2022).

[45] Carl Roth, Safety data sheet, Arachidic acid. https://shorturl.at/afjHQ. (Accessed on 23/11/2022).

[46] ThermoFisher SCIENTIFIC, Safety data sheet, Arachidic acid. https://rb.gy/xlriq. (Accessed on 23/11/2022).

[47] Mjallal, I., Feghali, E., Hammoud, M., Habchi, C., & Lemenand, T. Exploring the colligative properties of Arachidic acid for potential use as PCM. *Solar Energy*, 214: 19-25, 2021.

[48] Zhang, S., Wu, W., & Wang, S. Integration highly concentrated photovoltaic module exhaust heat recovery system with adsorption air-conditioning module via phase change materials. *Energy*, 118: 1187-1197, 2017.

[49] El-Sebaii, A. A., Al-Heniti, S., Al-Agel, F., Al-Ghamdi, A. A., & Al-Marzouki, F. One thousand thermal cycles of magnesium chloride hexahydrate as a

promising PCM for indoor solar cooking. *Energy Conversion and Management*, 52(4):1771-1777, 2011.

[50] Sharma, A., Sharma, S. D., & Buddhi, D. Accelerated thermal cycle test of acetamide, stearic acid and paraffin wax for solar thermal latent heat storage applications. *Energy Conversion and Management*, 43(14):1923-1930, 2002.

[51] Emons, H. H., Naumann, R., Jahn, K., & Flammersheim, H. J. Thermal properties of acetamide in the temperature range from 298 K to 400 K. *Thermochimica acta*, 104:127-137, 1986.

[52] Sharma, S. D., Buddhi, D., Sawhney, R. L., & Sharma, A. Design, development and performance evaluation of a latent heat storage unit for evening cooking in a solar cooker. *Energy Conversion and Management*, 41(14):1497-1508, 2000.

[53] Cabeza, L. F., Roca, J., Nogués, M., Mehling, H., & Hiebler, S. Immersion corrosion tests on metal-salt hydrate pairs used for latent heat storage in the 48 to 58° C temperature range. *Materials and corrosion*, 53(12):902-907, 2002.

[54] Cabeza, L. F., Roca, J., Noguees, M., Mehling, H., & Hiebler, S. Long term immersion corrosion tests on metal-PCM pairs used for latent heat storage in the 24 to 29° C temperature range. *Materials and corrosion*, 56(1):33-39, 2005.